



PCCP

**Direct observation of the doorway  $1n\pi^*$  state  
of methylcinnamate and hydrogen-bonding effects on the  
photochemistry of cinnamate-based sunscreens**

Journal:	<i>Physical Chemistry Chemical Physics</i>
Manuscript ID	CP-ART-05-2019-002914.R1
Article Type:	Paper
Date Submitted by the Author:	14-Jun-2019
Complete List of Authors:	Kinoshita, Shin-nosuke; Hiroshima University Inokuchi, Yoshiya; Hiroshima University Onitsuka, Yuuki; Hiroshima University Kohguchi, Hiroshi; Hiroshima University Akai, Nobuyuki; Tokyo University of Agriculture and Technology Shiraogawa, Takafumi; SOKENDAI Ehara, Masahiro; Institute for Molecular Science Yamazaki, Kaoru; Tohoku University Harabuchi, Yu; Hokkaido University Maeda, Satoshi; Hokkaido University Ebata, Takayuki; Hiroshima University

SCHOLARONE™  
Manuscripts

## ARTICLE

# Direct observation of the doorway $^1n\pi^*$ state of methylcinnamate and hydrogen-bonding effects on the photochemistry of cinnamate-based sunscreens

Received 00th January 20xx,  
Accepted 00th January 20xx

DOI: 10.1039/x0xx00000x

Shin-nosuke Kinoshita,<sup>a</sup> Yoshiya Inokuchi,<sup>a</sup> Yuuki Onitsuka,<sup>a</sup> Hiroshi Kohguchi,<sup>a</sup> Nobuyuki Akai,<sup>b</sup> Takafumi Shiraogawa,<sup>c</sup> Masahiro Ehara,<sup>\*c, d</sup> Kaoru Yamazaki,<sup>\*e</sup> Yu Harabuchi,<sup>f, g, h</sup> Satoshi Maeda,<sup>f, h</sup> and Takayuki Ebata<sup>\*a</sup>

The electronic states and photochemistry including nonradiative decay (NRD) and *trans(E)* → *cis(Z)* isomerization of methylcinnamate (MC) and its hydrogen-bonded complex with methanol have been investigated under jet-cooled condition. The  $S_1(^1n\pi^*)$  and  $S_2(^1\pi\pi^*)$  are directly observed in MC. This is the first direct observation of  $S_1(^1n\pi^*)$  among cinnamate derivatives. Surprisingly, the order of the energies between the  $n\pi^*$  and  $\pi\pi^*$  states is opposite to substituted cinnamates. TD-DFT and SAC-CI calculations support the observed result and show that the substitution to the benzene ring largely lowers the  $^1\pi\pi^*$  energy while the effect to  $^1n\pi^*$  is rather small. The  $S_2(^1\pi\pi^*)$  state lifetime of MC is determined to be equal to or shorter than 10 ps, and the production of the transient  $T_1$  state is observed. The  $T_1(^1\pi\pi^*)$  state is calculated to have the structure in which propenyl C=C is twisted by 90°, suggesting the *trans* → *cis* isomerization proceeds *via*  $T_1$ . The production of the *cis* isomer is confirmed by low-temperature matrix-isolated FTIR spectroscopy. The effect of the H-bonding is examined for the MC-methanol complex. The  $S_2$  lifetime of MC-methanol is determined to be 180 ps, indicating the H-bonding to the C=O group largely prohibits the  $^1\pi\pi^* \rightarrow ^1n\pi^*$  internal conversion. This lifetime elongation in methanol complex also describes well a higher fluorescence quantum yield of MC in methanol solution than in cyclohexane, while such the solvent dependence is not observed in *para*-substituted MC. Determination of the photochemical reaction pathways of MC and MC-methanol will help us to design photofunctional cinnamate derivatives.

## 1. Introduction

Cinnamic acids and cinnamates, ubiquitous alpha beta unsaturated acids and esters, are widely distributed in nature. Their photochemistry has been the subject for many years.<sup>1-44</sup> They take a stable *trans*-form in the electronic ground state ( $S_0$ ). After UV absorption, they immediately relax *via* several nonradiative decay (NRD) routes and finally go back either the *trans*- or isomerize to *cis*-form.<sup>1,19</sup> *Para*-coumaric acid (*p*-CA) is known as a chromophore in photoactive yellow protein (PYP) existing in *Halorhodospira*

*halophile*,<sup>1-5</sup> and cinnamate derivatives exist in the plants to protect damage of sunlight.<sup>6-13</sup> Because of the effective NRD process and transfer of the absorbed UV light to thermal energy, their derivatives are used as a sunscreen cosmetic reagent<sup>14-16</sup> and in pharmacology.<sup>17,18</sup> The UV spectroscopy of cinnamate derivatives and their photochemical characteristics have been reported extensively in solution as well as under protein environment.<sup>20-25</sup>

Gas-phase studies on the electronic states and photochemistry of cinnamates have been also extensively carried out under jet-cooled condition,<sup>26-34</sup> mostly for substituted cinnamates: *para*-substituted-cinnamates by Buma and coworkers,<sup>27-30</sup> ferulic and sinapic acids and their esters by the groups of Zwier and Stavros.<sup>31-34</sup> This is because those molecules are relevant to PYP, lignin and sunscreen cosmetic reagents. Especially, Stavros and co-workers carried out the gas-phase spectroscopy and time-resolved study in liquid-phase and discussed possible photoisomerization routes.<sup>35-39</sup>

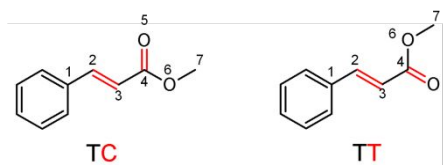


**Chart 1** Schematic Structure of TC and TT Conformers of Methylcinnamate (MC)

<sup>a</sup> Department of Chemistry, Graduate School of Science, Hiroshima University, Higashi-Hiroshima 739-8526, Japan. E-mail: [tebata@hiroshima-u.ac.jp](mailto:tebata@hiroshima-u.ac.jp)

<sup>b</sup> Graduate School of Bio-Applications and Systems Engineering (BASE), Tokyo University of Agriculture and Technology, Naka-cho, Koganei, Tokyo 184-8588, Japan

<sup>c</sup> SOKENDAI, the Graduate University for Advanced Studies, Myodaiji, Okazaki 444-8585, Japan

<sup>d</sup> Institute for Molecular Science and Research Center for Computational Science, 38, Myodaiji, Okazaki 444-8585, Japan. E-mail: [ehara@ims.ac.jp](mailto:ehara@ims.ac.jp)

<sup>e</sup> Institute for Materials Research, Tohoku University, Katahira 2-1-1, Aoba-ku, Sendai, 980-8577, Japan. E-mail: [kaoru.yamazaki@imr.tohoku.ac.jp](mailto:kaoru.yamazaki@imr.tohoku.ac.jp)

<sup>f</sup> Department of Chemistry, Faculty of Science, Hokkaido University, Sapporo 060-0810, Japan

<sup>g</sup> JST, PRESTO, 4-1-8 Honcho, Kawaguchi, Saitama, 332-0012, Japan

<sup>h</sup> Institute for Chemical Reaction Design and Discovery (WPI-ICReDD), Hokkaido University, Sapporo 001-0021, Japan

† Footnotes relating to the title and/or authors should appear here.

Electronic Supplementary Information (ESI) available: [details of any supplementary information available should be included here]. See DOI: 10.1039/x0xx00000x

Our group has also been studying the electronic states and photochemistry of substituted cinnamates by gas-phase laser spectroscopy and by the product analysis by cold matrix-isolated FTIR spectroscopy.<sup>19, 40-44</sup> We recently proposed the mechanism of the isomerization for the *para*-substituted cinnamates as “[*trans*]<sup>1</sup> $\pi\pi^*$ ]  $\rightarrow$  [<sup>1</sup> $n\pi^*$ ]  $\rightarrow$  [ $T_1$ ]  $\rightarrow$  [(*cis*) $S_0$ ]” by combining experiments and theoretical calculations.<sup>42</sup> The most important issue is the detection of the  $T_1(\pi\pi^*)$  state as the transient state by nanosecond ultraviolet (UV) - Deep UV (DUV) pump-probe spectroscopy.<sup>42</sup> We further examined the effect of the substitution position on the isomerization for the structural isomers of hydroxy methylcinnamate (HMC).<sup>43</sup> It was found that the isomerization of *m*- and *o*-HMC proceeds via different isomerization route from that of *p*-HMC. That is, in *m*- and *o*-HMC the barrier height of <sup>1</sup> $\pi\pi^* \rightarrow$  <sup>1</sup> $n\pi^*$  internal conversion (IC) is higher than *p*-HMC and the isomerization occurs via the “[*trans*]<sup>1</sup> $\pi\pi^*$ ]  $\rightarrow$  [twisting along the C=C double bond by 90° on  $S_1$ ]  $\rightarrow$  [(*cis*) $S_0$ ]” route.<sup>43</sup> The effect of hydrogen(H)-bonding on the NRD channel has been also investigated for *p*-HMC.<sup>40</sup> and *p*-methoxy methylcinnamate (*p*-MMC).<sup>41</sup> These results showed that the <sup>1</sup> $\pi\pi^*$  lifetime is very sensitive to the position of H-bonding. The important fact we know from these studies is that the <sup>1</sup> $\pi\pi^*$  and <sup>1</sup> $n\pi^*$  states are energetically close with each other in these molecules, and their energies change sensitively by the internal as well as external environments.

In spite of many studies reported for cinnamate derivatives, very few studies have been reported for methyl cinnamate (MC, chart 1), the simplest cinnamate ester. To the best of our knowledge, there is only one gas-phase study reported by Ebata *et al.*<sup>26</sup> They measured laser-induced fluorescence (LIF) and UV-UV hole-burning (UV-UV HB) spectra of jet-cooled MC and found the electronic transitions corresponding to two conformers (chart 1, TC and TT). In addition, they reported that the lifetimes of the vibronic bands drastically become shorter with the energy. However, they did not assign the observed electronic transitions. Determination of the photochemical reaction pathway and hydrogen bonding effects for MC, fundamental cinnamate, should help us to design cinnamate based bio-inspired photofunctional molecules.

In the present study, we carried out laser spectroscopic study for jet-cooled MC in wider energy region to reveal the electronic structure. In addition, we confirmed the *trans*  $\rightarrow$  *cis* photoisomerization by cold matrix-isolated FTIR experiment. The effect of the H-bonding on the C=O group has been also investigated for the 1:1 complex with methanol. Finally, we compared the absorption and fluorescence spectra of MC with *para*-substituted MC in methanol and cyclohexane solution at room temperature, and we found that the effect of the H-bonding can explain very well the solvent dependent fluorescence quantum yield of MC. The present study will be a very important step for the full understanding of the photochemistry of cinnamic acid and cinnamate family.

## 2. Experimental methods

The experimental setup for the laser spectroscopy of jet-cooled molecules in the gas phase has been described elsewhere.<sup>19, 40-44</sup> Briefly, a jet-cooling of MC was achieved by expanding the mixture

of vaporized MC and carrier gas (He) at the total pressure of 5 atm into a vacuum chamber by using a pulse nozzle. MC powder was heated to obtain enough vapor pressure. For generating MC-methanol (MeOH) complex, methanol vapor was mixed with the carrier gas. Two vacuum chambers were used for spectroscopy of jet-cooled MC. For the measurement of the LIF spectra, we used a free-jet expansion chamber. A tunable UV laser pulse was irradiated to the jet-cooled MC at 20 mm downstream of the nozzle and the total fluorescence was collected by a series of lenses and detected by photomultiplier tube (Hamamatsu Photonics 1P28). A band pass filter was used to eliminate the scatter of laser light. For the measurement of the resonance two-photon ionization (R2PI), we used the molecular beam chamber equipped with a 50 cm time-of-flight mass spectrometer. We adopted two-colour (2C)-R2PI ( $\nu_1$ ,  $\nu_2$ ), with frequency of  $\nu_2$  higher than  $\nu_1$ . This is due to the fact that the energies of both the  $S_1$  and  $S_2$  states are lower than half of the ionization potential (IP<sub>0</sub>) and higher frequency laser is necessary for the ionization step. This part will be described in the next section.

The lifetimes of the excited states were determined by observing the fluorescence decay profile or by picosecond UV-UV' pump-probe measurement. In the former, we used fast response photomultiplier tube (Hamamatsu Photonics R9880U) and the lifetimes were obtained by deconvolution assuming 5 ns laser pulse width (FWHM). In the latter, two tunable picosecond laser pulses (Ekspra PL2143S/PG401SH) with the pulse width (FWHM) of 12 ps were used. The first laser ( $\nu_1$ ) pumps the molecules to the vibronic level of the excited state, and second laser ( $\nu_2$ ) ionizes the excited molecules, and the delay time between two laser pulses was controlled by an optical delay line. The decay profile of the excited molecules was analysed by deconvolution.

For nanosecond UV-DUV pump-probe measurement, a tunable DUV light was generated by sum frequency mixing (SFG) between the second harmonics of the Nd:YAG laser pumped dye laser and the fundamental (1.064  $\mu\text{m}$ ) of the same Nd:YAG laser. The decay profile was analysed by deconvolution with the laser pulse width (FWHM) of 5 ns.

In the low temperature matrix-isolated FTIR spectroscopic study, vaporized MC is mixed with Ne and deposited on a CsI plate cooled at 6 K.<sup>19</sup> The IR spectrum of the Ne-matrix isolated MC was measured by FTIR spectrophotometer (JEOL SPX200ST) with 0.5  $\text{cm}^{-1}$  spectral resolution. A Xe lamp was used as UV light source. The photoproducts were analysed by subtracting the IR spectrum of the UV irradiated sample from that without UV irradiation.

For the measurement of the UV absorption spectra of MC in methanol and cyclohexane solution, a commercial spectrophotometer (Hitachi U-3010) was used. The fluorescence spectra of MC in the solutions were measured with a fluorescence spectrophotometer (Hitachi F-2500). The concentration of solution was set in the order of  $10^{-4}$  M for the absorption and  $10^{-5}$  M for the fluorescence measurements.

## 3. Theoretical calculations

To assign the observed electronic transitions, we calculated the stable structure and adiabatic excitation energies by density functional theory (DFT), time-dependent DFT (TD-DFT) and symmetry-adapted cluster-configuration interaction (SAC-CI)

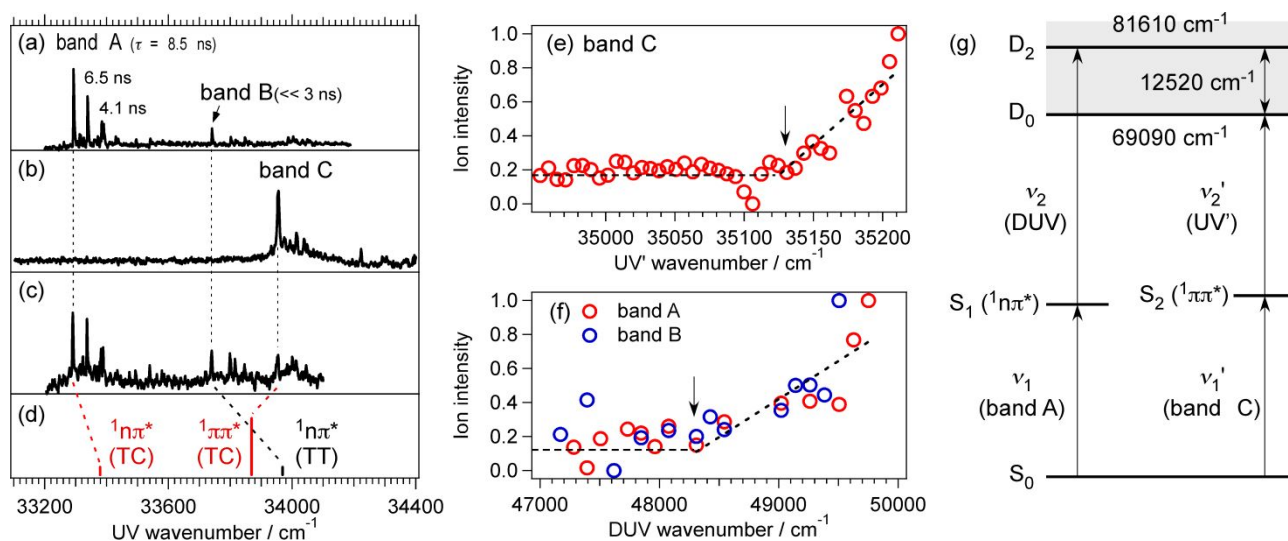


**Fig. 1.** (a) LIF spectrum of jet-cooled MC. (b) 2C-R2PI spectrum of jet-cooled MC with ionization laser at 205.75 nm, and (c) 202 nm, respectively. (d) ZPE corrected adiabatic excitation energy calculated at  $\omega$ B97X-D/6-311G(d, p) level. Here we used a scaling factor of 0.9725. Ionization efficiency curve from (e) band C, and (f) bands A and B. (g) Energy levels diagram of MC. The energies ( $D_0$  and  $D_2$ ) are experimentally obtained.

theory.<sup>45-49</sup> The  $S_0$  structures of MC, *p*-HMC and *p*-MMC were optimized using DFT, and the  $^1\pi\pi^*$  and  $^1n\pi^*$  structures were optimized using TD-DFT. Adiabatic excitation energies of the TC conformer at the TD-DFT level were evaluated with the zero-point energy (ZPE) correction. In the case of MC, the  $S_0$ ,  $^1\pi\pi^*$  and  $^1n\pi^*$  structures of the less stable conformer, i.e. TT, were also optimized, and the adiabatic excitation energies were compared with those of TC. The DFT and TD-DFT calculations were done using  $\omega$ B97X-D functional<sup>50</sup> with 6-311G(d, p) basis set ( $\omega$ B97X-D/6-311G(d, p)). Adiabatic excitation energies for  $^1\pi\pi^*$  and  $^1n\pi^*$  were also computed at the direct SAC-CI method<sup>51</sup> at Level five (Lv5) accuracy<sup>52, 53</sup> with 6-311G(d) basis set (SAC-CI/6-311G(d) level). Energies at the SAC-CI/6-311G(d) level were calculated on the geometries optimized at the DFT and TD-DFT levels.

To compare with the experimentally obtained ionization energies, the possible ionization energies were evaluated by calculating the lowest  $\pi^1$  and  $n^1$  states at the SAC-CI NV/6-311G(d, p) Lv 5 level with the geometries obtained by the Lv3 calculation.

**Table 1.** Observed electronic transitions and calculated ZPE-corrected adiabatic excitation energies ( $\text{cm}^{-1}$ ) (non-scaled) and characters of the two lowest singlet excited states of MC (TC), *p*-HMC (*anti* TC) and *p*-MMC (*anti* TC).

	MC		<i>p</i> -HMC		<i>p</i> -MMC		
	State	Energy ( $\text{cm}^{-1}$ )	$\Delta E$	Energy ( $\text{cm}^{-1}$ )	$\Delta E$	Energy ( $\text{cm}^{-1}$ )	$\Delta E$
Observed	$S_1$	33300 ( $n\pi^*$ )		32710 ( $\pi\pi^*$ )		32667 ( $\pi\pi^*$ )	
	$S_2$	33960 ( $\pi\pi^*$ )	660	-		-	
$\omega$ B97X-D/6-311G(d, p)	$S_1$	34323 ( $n\pi^*$ )		33697 ( $\pi\pi^*$ )		33368 ( $\pi\pi^*$ )	
	$S_2$	34827 ( $\pi\pi^*$ )	504	34692 ( $n\pi^*$ )	995	34743 ( $n\pi^*$ )	1375
SAC-CI/6-311G(d)	$S_1$	35765 ( $n\pi^*$ )					
	$S_2$	37621 ( $\pi\pi^*$ )	1856				

In addition, most stable structure of TC conformer of MC-MeOH was calculated at the  $\omega$ B97X-D/6-311G(d, p) level. The detailed structure of MC-MeOH is shown in Supporting Information (Figure S1).

All the energy, gradient, and Hessian calculations at the DFT, TD-DFT, and SAC-CI levels were done using Gaussian16 program package.<sup>54</sup>

## 4. Results and Discussion

### 4.1. Electronic spectra of jet-cooled Methylcinnamate

Figure 1 (a) shows the LIF spectrum of jet-cooled MC in the region from 33200 to 34200  $\text{cm}^{-1}$ . The spectral feature is essentially the same with that reported by Ebata *et al.*<sup>26</sup> As was reported, there are two electronic transitions in the spectrum. One is the vibronic bands in the 33300-33600  $\text{cm}^{-1}$  region with the band origin at 33300  $\text{cm}^{-1}$  (band A), and the other appears in the 33700-34100  $\text{cm}^{-1}$  region with

the band origin at  $33740\text{ cm}^{-1}$  (band B). As to these vibronic bands, Ebata *et al.* concluded that almost all the vibronic bands are assigned to the electronic transitions of the two conformers of MC by UV-UV hole-burning (HB) spectroscopy, but the assignment of the two conformers was not done at that time. Figures 1 (b) and (c) show the mass-selected 2C-R2PI spectra of MC obtained with the ionization wavelength of  $205.75\text{ nm}$  ( $48600\text{ cm}^{-1}$ ) and  $202.0\text{ nm}$  ( $49500\text{ cm}^{-1}$ ), respectively. The spectra were measured by the nanosecond laser, where the delay time between the pump and probe lasers is fixed at zero nanosecond. As seen in Figure 1 (b), neither band A nor band B is observed but a new strong band C emerged at  $33960\text{ cm}^{-1}$ . In Figure 1 (c), on the other hand, all the bands A, B, and C appeared. These results indicate that band C is the electronic state different from bands A and B, and such the state has not been observed in either *p*-HMC or *p*-MMC.

#### 4.2. Assignment of conformer and electronic transitions

To assign the observed electronic transitions of MC, we calculated stable structure and adiabatic excitation energies by DFT, TD-DFT and SAC-CI methods. The structures in  $S_0$ ,  ${}^1\pi\pi^*$  and  ${}^1n\pi^*$  and the adiabatic excitation energies were calculated at the  $\omega$ B97X-D/6-311G(d, p) and SAC-CI/6-311G(d) Lv5 level of theories. As was described above, MC has two conformers (TC and TT). Their structures and relative energies in  $S_0$  are shown in Supporting Information (Figure S1). In  $S_0$ , TC is most stable and TT is  $350\text{ cm}^{-1}$  higher.

The zero-point energy (ZPE) corrected adiabatic excitation energies of TC conformer are listed in Table 1. Also listed are the energies of the observed (0,0) band of each species. As seen in the table, both theoretical calculations predict the lowest singlet excited state to be  ${}^1n\pi^*$  and second to be  ${}^1\pi\pi^*$ . So, it is quite possible that bands A and B are assigned to the  ${}^1n\pi^*$  state of the two conformers of MC, and band C to the  ${}^1\pi\pi^*$  state. The obtained stable structures of the  $S_1({}^1n\pi^*)$  and  $S_2({}^1\pi\pi^*)$  states of the MC conformer are shown in Supporting Information (Figure S2). As seen in Figure S2,  $S_2({}^1\pi\pi^*)$  has a planar structure, while in  $S_1({}^1n\pi^*)$   $C_7$  is slightly tilted out-of-plane around the  $C_4$ - $C_6$  axis.

Since we expect two bands for the  ${}^1\pi\pi^*$  state corresponding two conformers, we also performed the geometry optimization for the  ${}^1\pi\pi^*$  and  ${}^1n\pi^*$  states of the TT conformer of MC and tried to calculate its 0-0 transition energies. However, we could obtain only the adiabatic energy of the  ${}^1n\pi^*$  state, and a stable structure was not found for the  $S_2({}^1\pi\pi^*)$  state in either  $\omega$ B97X-D/6-311G(d, p) level or SAC-CI/6-311G(d) level of theories for TT nearby its Franck-Condon region. Actually, the calculation at  $\omega$ B97X-D/6-311G(d, p) level shows that the  ${}^1\pi\pi^*$  state of TT is unstable and collapses into a conical intersection having a C=C twisted structure without experiencing any barrier. This is consistent with the experimental result that we observed only band C in the 2C-R2PI spectrum in Figure 1 (b). So, band C can be assigned to the  ${}^1\pi\pi^*$  state of the TC conformer. In this figure, there is a weak band at  $34210\text{ cm}^{-1}$ . It is not clear whether this band is the vibronic bands belonging to band C or the band origin of the TT conformer. Another possible reason of non-appearance of  $S_2({}^1\pi\pi^*)$  of the TT conformer is the short lifetime. As will be discussed later, the lifetime of band C is equal to or shorter than 10 ps. If the

band of TT has a shorter lifetime, the band intensity would be very weak in Figure 1 (b).

We then compare the adiabatic energies of the excited states between TC of MC and *anti*-TC conformer of *p*-HMC as well as *p*-MMC in Table 1. In both *p*-HMC and *p*-MMC, *anti*-TC is the most stable conformer in  $S_0$ .<sup>40,41</sup> The calculated results in this table show that the order of the energies between  ${}^1n\pi^*$  and  ${}^1\pi\pi^*$  of MC is opposite to that of *p*-HMC and *p*-MMC. Actually, in *p*-HMC and *p*-MMC, we observed only the  ${}^1\pi\pi^*$  state as  $S_1$  and the  ${}^1n\pi^*$  state was not observed, due to that the weak  $S_0 \rightarrow S_2({}^1n\pi^*)$  absorption is buried by the strong  $S_0 \rightarrow S_1({}^1\pi\pi^*)$  absorption in those molecules.<sup>38-42,55</sup> In the table, we can see clearly the effect of the substitution to phenyl ring on the electronic states; the energy of the  ${}^1\pi\pi^*$  state becomes lower upon the substitution, while that of the  ${}^1n\pi^*$  remain the same. Thus, it is quite possible that in MC the  ${}^1n\pi^*$  state is  $S_1$  and the  ${}^1\pi\pi^*$  state is  $S_2$ , and this is the reason why we could detect the  ${}^1n\pi^*$  state of MC. This finding is also commented in our previous paper on sinapic acid that the substitution to the phenyl ring lowers the  ${}^1\pi\pi^*$  energy while the energy of  ${}^1n\pi^*$  is less affected.<sup>44</sup>

For the secure assignment of the observed electronic transitions of MC, we measured the ionization energies from bands A, B and C. Figure 1 (e) shows the ionization efficiency curve from band C, and Figure 1 (f) shows that from bands A and B. In Figure 1 (e), an ionization threshold is seen at  $\nu_2 = 35130\text{ cm}^{-1}$ , corresponding to the ionization energy of  $69090\text{ cm}^{-1}$ . On the other hand, the ionization threshold from bands A and B is observed at  $\nu_2 = 48280\text{ cm}^{-1}$ . This energy is much higher than that of band C, and the ionization energy is obtained to be  $81610\text{ cm}^{-1}$ . The result means that bands A and B are correlated to the excited state of the ion. We then calculated the adiabatic ionization potential for  $D_0$ ,  $D_1(\pi^{-1})$  and  $D_2(n^{-1})$  at the SAC-CI-NV/6-311G(d, p) Lv5 level. The calculated  $D_0$  energy is  $67107\text{ cm}^{-1}$ , and  $D_2(n^{-1}) - D_0(\pi^{-1})$  energy gap is  $10767\text{ cm}^{-1}$ . The calculated  $D_0$  reasonably agrees with the obtained ionization energy from band C ( $69090\text{ cm}^{-1}$ ), and the  $D_2(n^{-1}) - D_0(\pi^{-1})$  gap also agrees that of the difference of the ionization energies from band A (band B) and band C,  $12520\text{ cm}^{-1}$ . Thus, the electronic state corresponding to band C is ionized to  $D_0(\pi^{-1})$  and band A (band B) to  $D_2(n^{-1})$ , and we conclude that the bands A and B are the band origins of the  ${}^1n\pi^*$  state of the TT and TC conformers, respectively, and band C to the origin of  ${}^1\pi\pi^*$  state of TC. Figure 1 (d) shows the scaled adiabatic excitation energies of MC for  $S_1({}^1n\pi^*)$  and  $S_2({}^1\pi\pi^*)$ . It should be noted this study is first case of the direct observation of the  ${}^1n\pi^*$  state among cinnamate family.

#### 4.3. Lifetime measurement and nonradiative decay process

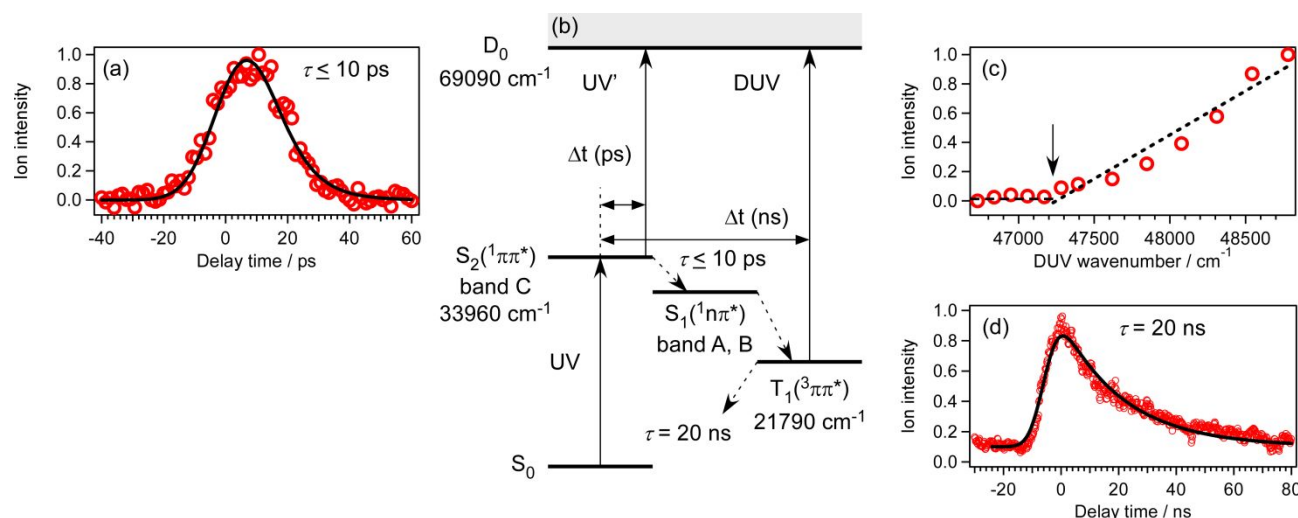


**Fig. 2** (a) Time profile of band C, observed by ps UV-UV' pump-probe spectroscopy. (b) Energy levels diagram of MC and excitation/relaxation schemes. (c) Ionization efficiency curve of the transient state observed by ns UV-Deep UV pump-probe spectroscopy, where the delay time is fixed at 15 ns. An arrow indicates the threshold of the ionization. (d) Time profile of the transient state ( $T_1$ ) observed by ns UV-Deep UV pump-probe spectroscopy.

We then measured the excited state lifetimes and investigated NRD route. In Figure 1 (a), the fluorescence decay lifetimes are given for "A (0,0)", "(0,0) + 46  $\text{cm}^{-1}$ ", "(0,0) + 92  $\text{cm}^{-1}$ " and "B (0,0)" bands. The observed decay profiles are shown in Supporting Information (Figure S3). The fluorescence lifetimes of higher vibronic bands rapidly become short and those above 33400  $\text{cm}^{-1}$  are too short to be obtained. This result indicates that intersystem crossing (ISC) channel to the  $T_1$  state is open even at low energy region of the  $S_1(1n\pi^*)$  state.

We next discuss the NRD from the  $S_2(1\pi\pi^*)$  state. Figure 2 (a) shows time profile of band C obtained by picosecond (ps) UV-UV' pump-probe spectroscopy. Here,  $\nu_1$  and  $\nu_2$  are fixed to band C and 41140  $\text{cm}^{-1}$  (243.1 nm), respectively. The time profile was the same even if we used different ionization laser frequencies ( $\nu_2$ ), indicating the profile to be the decay of band C. The red circles are observed pump-probe ion signals and the black solid curve are convoluted decay curve fitted by assuming a single exponential decay of  $\tau = 10$  ps with laser pulse width (FWHM) of 12 ps. This lifetime is the shortest one that we can obtain with our ps laser system so that true lifetime may be shorter than 10 ps. This short lifetime means that the  $S_2(1\pi\pi^*)$  lifetime can be controlled mainly by internal conversion (IC) to  $S_1(1n\pi^*)$ .

We further applied nanosecond (ns) UV-Deep UV pump-probe spectroscopy to detect the transient state produced after the decay of  $S_2$ . Figure 2 (b) shows the ionization efficiency curve of the transient state. Here,  $\nu_1$  is fixed at band C and  $\nu_2$  is scanned, with delay time  $\Delta t = 15$  ns. The ion intensity gradually increases at  $\nu_2 \sim 47300 \text{ cm}^{-1}$ . By assuming that the transient state can be ionized to  $D_0$  and using the experimentally obtained  $D_0$ , we determined the energy of the transient state to be 21790  $\text{cm}^{-1}$ . This value is similar to those of the  $T_1(3\pi\pi^*)$  state of *p*-HMC (19020  $\text{cm}^{-1}$ )<sup>43</sup> and *p*-MMC (16577  $\text{cm}^{-1}$ )<sup>42</sup> reported in our previous papers. In addition, Herkstroeter and Farid reported the  $T_1$  energy of MC to be 54.8  $\text{kcal}\cdot\text{mol}^{-1}$  (19170  $\text{cm}^{-1}$ ) by T-T transfer in solution.<sup>56</sup> Their value is also in good agreement

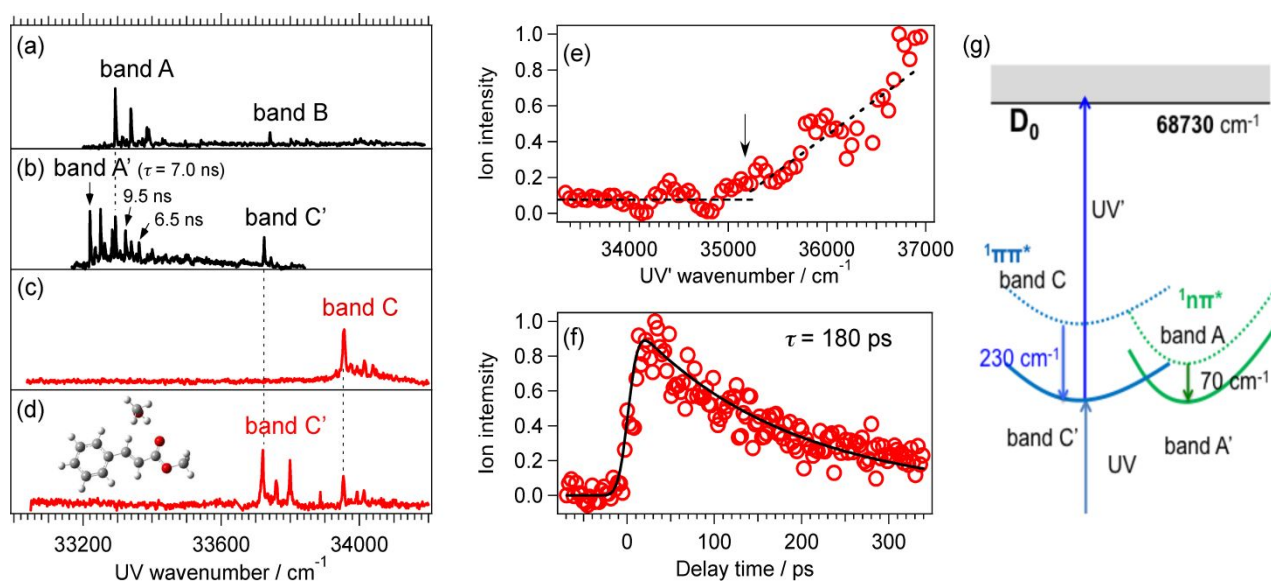
with that of the present transient state. We calculated the structure of the  $T_1$  state at  $\omega\text{B97X-D/6-311G(d,p)}$  level. The calculated  $T_1$  has the  $\pi\pi^*$  character and the 0,0 transition energy is obtained to be 17751  $\text{cm}^{-1}$ . Although this value is a little bit smaller than the experimental one, we can assign the transient state to be  $T_1(3\pi\pi^*)$ .

Figure 2 (d) shows time profile of the  $T_1(3\pi\pi^*)$  state, where  $\nu_1$  is fixed at 33960  $\text{cm}^{-1}$  (band C) and  $\nu_2$  is set at 49260  $\text{cm}^{-1}$  (203.0 nm) respectively. The deconvolution of the decay curve fitted by a single exponential decay gives a lifetime of  $\tau = 20$  ns. This lifetime is comparable to those of *p*-HMC (24 ns)<sup>43</sup> and *p*-MMC (20-27 ns).<sup>42</sup> Figure 2 (b) shows the energy level diagram and excitation/relaxation scheme of MC. As seen in Figure S2,  $T_1(3\pi\pi^*)$  has the structure in which the dihedral angle between  $C_1$ - $C_2$  and  $C_3$ - $C_4$  is rotated by 90.2°, suggesting the transient structure for the isomerization. From these results, it is concluded that the NRD route of MC from  $S_2(1\pi\pi^*)$  is " $S_2(1\pi\pi^*) \rightarrow S_1(1n\pi^*) \rightarrow T_1(3\pi\pi^*) \rightarrow S_0(\text{trans or cis})$ ", similar to other *para*-substituted cinnamates.<sup>42, 43</sup>

#### 4.4. Effect of hydrogen-bonding on the energies and lifetimes of the excited states

The effect of H-bonding on the electronic structure and NRD of MC has been also investigated by generating the 1:1 cluster with methanol (MC-MeOH). Figures 3 (a) and (c) show the LIF and 2C-R2PI spectra of bare MC, respectively, and (b) and (d) show the LIF and 2C-R2PI spectra of the MC-MeOH complex measured by adding methanol vapor. Here, the ionization laser (UV') is fixed to 205.75 nm (48600  $\text{cm}^{-1}$ ) in both measurements. At this UV' frequency, an extensive fragmentation occurs for MC-MeOH after the ionization, so that we collected the sum of ion signal of the masses of MC and MC-MeOH in Figure 3 (d).

In Figure 3 (b), vibronic bands with the origin of A' at 33220  $\text{cm}^{-1}$  and band C' at 33720  $\text{cm}^{-1}$  emerged. The LIF spectrum of (b) is



**Fig. 3.** LIF spectrum of (a) bare MC, and (b) MC-MeOH (1:1) complex. The fluorescence lifetimes of several bands are also shown in (b). 2C-R2PI spectrum of bare (c) MC and (d) MC-MeOH (1:1) complex. Here, a sum of the masses of MC-MeOH and bare MC are plotted in (d) (see text). (e) Ionization efficiency curve from band C'. (f) ps pump-probe time profile of band C'. (g) Schematic potential curves of  ${}^1\pi\pi^*$  and  ${}^1n\pi^*$  of MC and MC-MeOH (1:1) complex (see text).

essentially the same with that reported by Ebata et al.,<sup>26</sup> and the appeared bands are assigned to the MC-MeOH 1:1 complex. Band A' is  $70\text{ cm}^{-1}$  red-shifted from band A of bare MC. This band is not observed in 2C-R2PI spectrum of Figure 3 (d), so that we assign band A' to the origin of the  ${}^1n\pi^*$  state.

On the other hand, band C' appeared in Figure 3 (b) also strongly appears in Figure 3 (d), so that this band is assigned to the origin of the  ${}^1\pi\pi^*$  state, which is  $230\text{ cm}^{-1}$  red-shifted from band C. The reason of the appearance of band C' in the LIF spectrum will be soon discussed. Figure 3 (e) shows the ionization efficiency curve from band C'. A threshold is seen at  $\nu_{UV'} = 35200\text{ cm}^{-1}$ , and the ionization potential of the cluster is obtained to be  $68730\text{ cm}^{-1}$ . This value is  $360\text{ cm}^{-1}$  lower than that of MC ( $69090\text{ cm}^{-1}$ ). The rather small difference of  $D_0$  values between them can be described as follows. In the MC-MeOH, methanol is H-bonded to lone-pair electron of C=O group of MC, while the ionization is the removal of the  $\pi$ -electron of phenyl group, so that the H-bonding to C=O will not affect on this ionization process. The calculated  $D_0$  energy is  $70260\text{ cm}^{-1}$  and this value reasonably agrees with the observed one ( $68730\text{ cm}^{-1}$ ). In addition, the most stable structure of MC-MeOH calculated at  $\omega$ B97X-D/6-311G(d, p) level is shown in Figure 3 (d) and detailed structure is shown in Supporting Information (Figure S1). As is expected, the OH group of MeOH is H-bonded to the C=O as a proton donor and the oxygen of MeOH is bonded to CH of the propenyl group. This structure is very similar to  $p$ -MMC-H<sub>2</sub>O reported in our previous study<sup>41</sup>. In  $p$ -MMC-H<sub>2</sub>O, the  ${}^1\pi\pi^*$  transition of  $p$ -MMC-H<sub>2</sub>O is red-shifted by  $\sim 200\text{ cm}^{-1}$  from bare  $p$ -MMC.

To investigate the H-bonding effect on NRD process, we measured fluorescence lifetime of MC-MeOH for the  ${}^1n\pi^*$  state in Figure 3 (b) and the  ${}^1\pi\pi^*$  state in Figure 3 (e). The decay profiles of the vibronic bands of the  ${}^1\pi\pi^*$  state are shown in Supporting Information (Figure S4). The lifetime of  ${}^1n\pi^*$  state in MC-MeOH at  $\nu = 0$  level (band A') is  $7.0\text{ ns}$  and almost same with that of bare MC

(band A). However, the lifetimes of the vibronic bands show little excess energy dependence. This result suggests that the H-bonding at the C=O group inhibits the  ${}^1n\pi^* \rightarrow T_1$  ISC. Figure 3 (e) shows the lifetime measurement of band C' by ps pump-probe spectroscopy. The  $243.1\text{ nm}$  ( $41140\text{ cm}^{-1}$ ) is used for the ionization. The deconvolution of the decay profile fitted by a single exponential decay gives a lifetime  $\tau = 180\text{ ps}$ . Thus, the  $S_2({}^1\pi\pi^*)$  lifetime of MC-MeOH is more than 18 times longer than bare MC, indicating that the H-bonding to the C=O group suppresses the " ${}^1\pi\pi^* \rightarrow {}^1n\pi^*$ " IC. This is the reason why band C' appeared in the LIF spectrum of Figure 3 (b). The suppression of IC in the complex is understood by that the stabilization energy of  ${}^1\pi\pi^*$  by H-bonding ( $230\text{ cm}^{-1}$ ) is larger than that of  ${}^1n\pi^*$  ( $70\text{ cm}^{-1}$ ), so that the barrier height of  ${}^1\pi\pi^* \rightarrow {}^1n\pi^*$  IC becomes higher than bare MC as shown schematically in Figure 3 (g).

#### 4.5. Fluorescence spectra of MC and $p$ -MMC in solution

The finding of above gas-phase experiment suggests that the fluorescence of MC in methanol solution will be stronger than that in nonpolar solvent. So we examined this expectation for MC in solution and compared with those of  $p$ -MMC and  $p$ -HMC.

Left panel of Figure 4 (a) shows the absorption spectrum of MC and  $p$ -MMC in cyclohexane solution, and that of Figure 4 (b) the absorption spectrum of MC,  $p$ -MMC, and  $p$ -HMC in methanol solution. The absorption spectrum of  $p$ -HMC in cyclohexane could not be obtained due to the low solubility under the experimental condition with the concentration of  $10^{-3}\text{ M}$ . The absorption in the 250-350 nm region is attributed to the  $S_0 \rightarrow {}^1\pi\pi^*$  transition. As seen in the spectra, the absorption intensity is almost the same for the three molecules, irrespective of the solvent. Right panel of Figure 4 (b) shows the fluorescence spectra of MC and  $p$ -MMC. As seen in the spectra, the fluorescence intensity of MC is four times weaker than that of  $p$ -MMC. This situation differs in methanol. The fluorescence intensity of MC at right panel of Figure 4 (b) is half of  $p$ -MMC or  $p$ -

HCM. That is, the fluorescence intensity of MC in methanol solution is two times stronger than that in cyclohexane. However, such the solvent dependence is not seen in *p*-MMC. The weakness of the fluorescence of MC in cyclohexane is due to that cyclohexane is a non-polar solvent so that the  $^1n\pi^*$  state is thought to be ally lower than that of the  $^1\pi\pi^*$  state. In this case, MC excited to the optically bright  $^1\pi\pi^*$  state will relax immediately to  $^1n\pi^*$  by IC and become

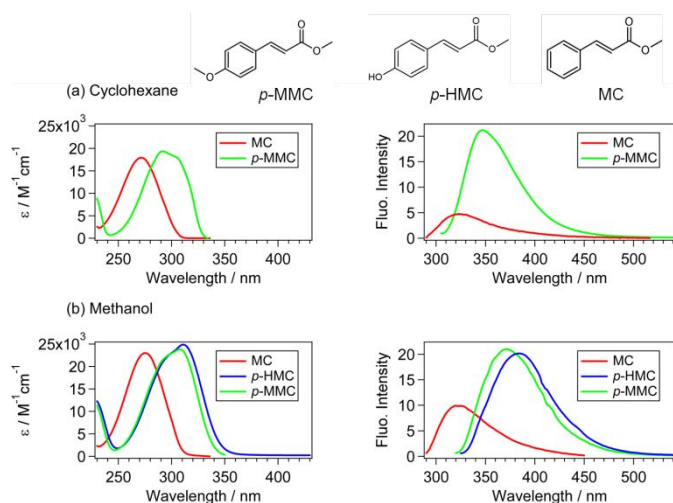


**Fig. 4.** (a) (left) Absorption spectra of MC and *p*-MMC in cyclohexane solution at room temperature. (right) Fluorescence spectra of MC and *p*-MMC measured by exciting their absorption maxima. The concentration is  $10^{-4}$  M in both measurements. (b) (left) Absorption spectra of MC, *p*-HMC, and *p*-MMC in methanol solution at room temperature. (right) Fluorescence spectra of MC, *p*-HMC, and *p*-MMC measured by exciting the absorption maximum of each species. The concentration is  $10^{-4}$  M for all the measurements.

less-fluorescent. On the other hand, the gas-phase experiment revealed that the H-bonding of methanol to the C=O group of MC prohibits the " $^1\pi\pi^* \rightarrow ^1n\pi^*$ " IC. Thus, the  $^1\pi\pi^*$  state of MC becomes more fluorescent in methanol solution. Such the solvent effect does not occur in *p*-MMC or *p*-HMC. This is because the adiabatic energy of  $^1\pi\pi^*$  is lower than  $^1n\pi$  in these molecules as seen in Table 1, and the H-bonding does not change this order. Actually, we observed that the H-bonding of H<sub>2</sub>O to the C=O group shorten the  $^1\pi\pi^*$  lifetime in *p*-MMC.<sup>41</sup> Thus, the situation of IC *p*-MMC and *p*-HMC may be similar in two solutions.

#### 4.6. Cold matrix-isolated FTIR experiment

In addition to above study, we carried out low temperature matrix isolated FTIR spectroscopy in order to identify the photoproduct after UV irradiation of MC. All of the FTIR spectra are shown in Supporting Information (Figure S5). By measuring the difference FTIR spectrum of MC before and after the UV irradiation at  $\lambda_{UV} > 300$  nm, we confirmed the production of *cis*-isomer after the UV irradiation to *trans*-MC by identifying its typical vibrations, such as propenyl C=C

stretching at  $1640\text{ cm}^{-1}$ . Therefore, it is clear that the *trans*  $\rightarrow$  *cis* photoisomerization occurs in MC after UV irradiation, similar to the cases of *p*-MMC<sup>19</sup> and HMC.<sup>43</sup>

## Conclusions

The electronic states and NRD process of bare MC and MC-MeOH complex have been investigated under jet-cooled gas phase condition. In the LIF spectrum, two transitions with the origin bands A and B, were observed and are assigned to the  $S_0 \rightarrow S_1(^1n\pi^*)$  transition of TC and TT conformers, respectively. While in 2C-R2PI spectra, a new band C appeared at higher frequency region, which is assigned to the  $S_2(^1\pi\pi^*)$  of the TC conformer. From the lifetime measurement, we found that  $S_1(^1n\pi^*)$  decays to  $T_1$  by ISC even at low energy ( $\sim 50\text{ cm}^{-1}$ ). The 0,0 band of  $S_2(^1\pi\pi^*)$  (band C) decays within 10 ps to  $S_1$  by IC and relaxes *via* the " $S_2(^1\pi\pi^*) \rightarrow S_1(^1n\pi^*) \rightarrow T_1(^3\pi\pi^*) \rightarrow S_0$ " route. The  $S_2(^1\pi\pi^*)$  lifetime is elongated more than 18 times in MC-MeOH complex, indicating the H-bonding to the C=O group of MC prohibits the " $S_2(^1\pi\pi^*) \rightarrow S_1(^1n\pi^*)$ " IC. This effect leads to the larger fluorescence quantum yield of MC in methanol solution than in cyclohexane solution.

From the present study and our previous studies, it is found that the substitution to the phenyl group considerably changes the relative energy between  $^1\pi\pi^*$  and  $^1n\pi^*$  of cinnamates although all the species exhibit *trans*  $\rightarrow$  *cis* isomerization. In our previous paper, we showed that the *trans*  $\rightarrow$  *cis* isomerization occurs *via* different routes in the structural isomers in HMC.<sup>43</sup> In that sense, the isomerization seems to be a robust reaction occurring with different manner in different kind of cinnamates. Finally, the present study on the photochemical behavior of cinnamates will provide a useful guideline to design photofunctional cinnamate derivatives.

## Conflicts of interest

The authors declare no competing financial interest.

## Acknowledgements

T. E. acknowledges the financial support from the Institute for Quantum Chemical Exploration, and the support by JSPS KAKENHI with Grant Number JP19K05387. K. Y. is grateful for the financial support from Building of Consortia for the Development of Human Resources in Science and Technology, MEXT. M. E. acknowledges the support by JSPS KAKENHI with Grant Numbers 16H06511 and 16H04104. Y. H. was supported by JST, PRESTO with Grant Number JPMJPR16N8. S. M. was supported by JST, CREST with Grant Number JPMJCR14L5. Y. I. acknowledges support by JSPS KAKENHI with Grant Number JP16H04098. H. K. acknowledges support by JSPS KAKENHI with Grant Number JP15KT0065.

## Notes and references

- 1 H. El-Gezawy, W. Rettig, A. Danel and G. Jonusauskas, *J. Phys. Chem. B*, 2005, **109**, 18699–18705.
- 2 T. E. Meyer, G. Tollin, T. P. Causgrove, P. Cheng and R. E. Blankenship, *Biophys. J.*, 1991, **59**, 988–991.
- 3 M. Baca, G. E. O. Borgstahl, M. Boissinot, P. M. Burke, D. R. Williams, K. A. Slater and E. D. Getzoff, *Biochemistry*, 1994, **33**, 14369–14377.
- 4 W. W. Sprenger, W. D Hoff, J. P Armitage and K. J. Hellingwerf, *J. Bacteriol.*, 1993, **175**, 3096–3104.
- 5 Y. Imamoto, M. Kataoka and F. Tokunaga, *Biochemistry*, 1996, **35**, 14047–14053.
- 6 Z. M. de Freitas, E. P. dos Santos, J. F. da Rocha, G. M. Dellamora-Ortiz, J. C. Gonçalves, *Eur. J. Pharm. Sci.*, 2005, **25**, 67–72.
- 7 P. K. Goswami, M. Samant, R. Srivastava, *Sch. Acad. J. Pharm.*, 2013, **2**, 458–463
- 8 R. Shuab, R. Lone, K.K. Koul, *Acta. Physiol. Plant*, 2016, **38**, 64–69
- 9 M. M. Caldwell, J. F. Bornman, C. L. Ballare, S. D. Flint, G. Kulandaivelu, *Photochem. Photobiol. Sci.*, 2007, **6**, 252–266.
- 10 G. I. Jenkins, *Ann. Rev. Plant Biol.* 2009, **60**, 407–431.
- 11 M. Tevini, A. H. Teramura, *Photochem. Photobiol.* 1989, **50**, 479–487.
- 12 H. Frohnmeyer, D. Staiger, *Plant Physiol.* 2003, **133**, 1420–1428.
- 13 J. Li, T. -M. Ou-Lee, R. Raba, R. G. Amundson, R. L. Last, *Plant Cell*, 1993, **5**, 171–179
- 14 M. S. Latha, J. Martis, V. Shobha, R. S. Shinde, S. Banger, B. Krishnankutty, S. Bellary, S. Varughese, P. Rao, B. R. N. Kumar, *J. Clin. Aesthet. Dermatol.* 2013, **6**, 16–26.
- 15 P. Perugini, M. Vettor, R. Tursilli, S. Scolio, I. Genta, T. Modena, F. Pavanetto, B. Conti, *J. Appl. Cosmetol.* 2005, **23**, 59–69
- 16 M. Nakajima, T. Kawakami, T. Niino, Y. Takahashi, S. Onodera, *J. Health Sci.*, 2009, **55**, 363–372
- 17 R. Lone, R. Shuab, K.K. Koul, *Global J. Pharmacol.*, 2014, **8**, 328–335,
- 18 A. Peperidou, I. Foropoulos, D. H-Litina, *Curr. Pharmace. Biotech.*, 2018, **19**, 1019–1048
- 19 Y. Miyazaki, Y. Inokuchi, N. Akai and T. Ebata, *J. Phys. Chem. Lett.*, 2015, **6**, 1134–1139.
- 20 J. Luo, Y. Liu, S. Yang, A. L. Flourat, F. Allais and K. Han, *J. Phys. Chem. Lett.*, 2017, **8**, 1025–1030.
- 21 D. S. Larsen, M. Vengris, I. H. M. van Stokkum, M. A. van der Horst, R. A. Cordfunke, K. J. Hellingwerf and R. van Grondelle, *Chem. Phys. Lett.*, 2003, **369**, 563–569.
- 22 J. Tenboer, S. Basu, N. Zatspein, K. Pande, K. D. Milathianaki, M. Frank, M. Hunter, S. Boutet, G. J. Williams, J. E. Koglin et al., *Science*, 2014, **346**, 1242–1246.
- 23 K. Pande, C. D. M. Hutchison, G. Groenhof, A. Aquila, J. S. Robinson, J. Tenboer, S. Basu, S. Boutet, D. P. DePonte, M. Liang, et al., *Science*, 2016, **352**, 725–729.
- 24 H. Kuramochi, S. Takeuchi, K. Yonezawa, H. Kamikubo, M. Kataoka, T. Tahara, *Nature Chem.*, 2017, **9**, 660–666
- 25 Y. Peperstraete, M. Staniforth, L. Baker, N. D. N. Rodrigues, N. C. Cole-Filipiak, W. Quan and V. G. Stavros, *Phys. Chem. Chem. Phys.*, 2016, **18**, 28140–28149.
- 26 T. Ebata, K. Saito, H. Ishikawa, and N. Mikami, *Res. Chem. Intermed.*, 1998, **24**, 803–812
- 27 S. Smolarek, A. Vdovin, E. M. M. Tan, M. de Groot, W. J. Buma, *Phys. Chem. Chem. Phys.*, 2011, **13**, 4393–4399.
- 28 E. M. M. Tan, S. Amirjalayer, S. Smolarek, A. Vdovin and W. J. Buma, *J. Phys. Chem. B*. 2013, **117**, 4798–4805.
- 29 E. M. M. Tan, S. Amirjalayer, B. H. Bakker and W. J. Buma, *Faraday Discuss.*, 2013, **163**, 321–340.
- 30 E. M. M. Tan, S. Amirjalayer, B. H. Bakker, and W. J. Buma, *J. Phys. Chem. Lett.*, 2014, **5**, 2464–2468.
- 31 C. P. Rodrigo, W. H. James, and T. S. Zwier, *J. Am. Chem. Soc.*, 2011, **133**, 2632–2614.
- 32 J. C. Dean, R. Kusaka, P. S. Walsh, F. Allais and T. S. Zwier, *J. Am. Chem. Soc.*, 2014, **136**, 14780–14795.
- 33 N. D. N. Rodrigues, M. Staniforth, J. D. Young, Y. Peperstraete, N. C. Cole-Filipiak, J. R. Gord, P. S. Walsh, D. M. Hewett, T. S. Zwier and V. G. Stavros, *Faraday Discuss.*, 2016, **194**, 709–729.
- 34 N. D. N. Rodrigues, M. Staniforth, V. G. Stavros, *Proc. R. Soc. London, Ser. A*, 2016, **472**, 2195.
- 35 L. A. Baker, M. D. Horbury, S. E. Greenough, F. Allais, P. S. Walsh, S. Habershon, A. G. Stavros, *J. Phys. Chem. Lett.*, 2016, **7**, 56–61
- 36 M. D. Horbury, L. A. Baker, W.-D. Quan, S. E. Greenough, A. G. Stavros, *Phys. Chem. Chem. Phys.* 2016, **18**, 17691–17697
- 37 L. A. Baker, B. Marchetti, T. N. V. Karsili, V. G. Stavros, M. N. R. Ashfold, *Chem. Soc. Rev.*, 2017, **46**, 3770–3791
- 38 L. A. Baker and V. G. Stavros, *J. Sci. Prog.*, 2016, **99**, 282–311
- 39 N. D. N. Rodrigues and V. G. Stavros *Science Progress*, 101 (2018) 8–31
- 40 D. Shimada, R. Kusaka, Y. Inokuchi, M. Ehara and T. Ebata, *Phys. Chem. Chem. Phys.*, 2012, **14**, 8999–9005.
- 41 Y. Miyazaki, K. Yamamoto, J. Aoki, T. Ikeda, Y. Inokuchi, M. Ehara and T. Ebata, *J. Chem. Phys.*, 2014, **141**, 244313.
- 42 K. Yamazaki, Y. Miyazaki, Y. Harabuchi, T. Taketsugu, S. Maeda, Y. Inokuchi, S. Kinoshita, M. Sumida, Y. Onitsuka, H. Kohguchi, M. Ehara, and T. Ebata, *J. Phys. Chem. Lett.*, 2016, **7**, 4001–4007.
- 43 S. Kinoshita, Y. Miyazaki, M. Sumida, Y. Onitsuka, H. Kohguchi, Y. Inokuchi, N. Akai, T. Shiraogawa, M. Ehara, K. Yamazaki, Y. Harabuchi, S. Maeda, T. Taketsugu and T. Ebata, *Phys. Chem. Chem. Phys.*, 2018, **20**, 17585–17598.
- 44 S. Kenjo, Y. Iida, N. Chaki, S. Kinoshita, Y. Inokuchi, K. Yamazaki, T. Ebata, *Chem. Phys.* 2018, **515**, 381–386
- 45 H. Nakatsuji, *Chem. Phys. Lett.*, 1978, **59**, 362–364.
- 46 H. Nakatsuji, *Chem. Phys. Lett.*, 1979, **67**, 334–342.
- 47 H. Nakatsuji, *Chem. Phys. Lett.*, 1979, **67**, 329–333.
- 48 H. Nakatsuji, *Acta Chim. Hung.*, 1992, **129**, 719–776.
- 49 M. Ehara, J. Hasegawa and H. Nakatsuji, *SAC-CI Method Applied to Molecular Spectroscopy, in Theory and Applications of Computational Chemistry: The First 40 Years*, ed. C. E. Dykstra, G. Frenking, K. S. Kim and G. E. Scuseria, Elsevier, Oxford, 2005, pp. 1099–1141.
- 50 J. D. Chai, M. Head-Gordon, *Phys. Chem. Chem. Phys.*, 2008, **10**, 6615–6620.
- 51 R. Fukuda and H. Nakatsuji, *J. Chem. Phys.*, 2008, **128**, 94105.
- 52 R. Fukuda and M. Ehara, *J. Comput. Chem.*, 2014, **35**, 2163–2176.
- 53 R. Fukuda and M. Ehara, *Theor. Chem. Acc.*, 2016, **135**, 105.
- 54 M. J. Frisch, G. W. Trucks, H. B. Schlegel, G. E. Scuseria, M. A. Robb, J. R. Cheeseman, G. Scalmani, V. Barone, G. A. Petersson, H. Nakatsuji, X. Li, M. Caricato, A. V. Marenich, J. Bloino, B. G. Janesko, R. Gomperts, B. Mennucci, H. P. Hratchian, J. V. Ortiz, A. F. Izmaylov, J. L. Sonnenberg, D. Williams-Young, F. Ding, F. Lipparini, F. Egidi, J. Goings, B. Peng, A. Petrone, T. Henderson, D. Ranasinghe, V. G. Zakrzewski, J. Gao, N. Rega, G. Zheng, W. Liang, M. Hada, M. Ehara, K. Toyota, R. Fukuda, J. Hasegawa, M. Ishida, T. Nakajima, Y. Honda, O. Kitao, H. Nakai, T. Vreven, K. Throssell, J. A. Montgomery, Jr., J. E. Peralta, F. Ogliaro, M. J. Bearpark, J. J. Heyd, E. N. Brothers, K. N. Kudin, V. N. Staroverov, T. A. Keith, R. Kobayashi, J. Normand, K. Raghavachari, A. P. Rendell, J. C. Burant, S. S. Iyengar, J. Tomasi, M. Cossi, J. M. Millam, M. Klene, C. Adamo, R. Cammi, J. W. Ochterski, R. L. Martin, K. Morokuma, O. Farkas, J. B. Foresman, and D. J. Fox, *Gaussian 16*, Gaussian, Inc., Wallingford CT, 2016.
- 55 J. Moon, H. Baek, J. S. Lim, and J. Kim, *Bull. Korean Chem. Soc.*, 2018, **39**, 427–434.
- 56 W. G. Herkstroeter and S. Farid, *J. Photochem.*, 1986, **35**, 71–85.

TOC figure

